New Results from CERES

H. Appelshäuser for the CERES Collaboration*:

D. Adamová[a], G. Agakichiev[b], H. Appelshäuser[c], V. Belaga[d], P. Braun-Munzinger[b], A. Cherlin[e], S. Damjanović[c], T. Dietel[c], L. Dietrich[c], A. Drees[f], S. I. Esumi[c], K. Filimonov[c], K. Fomenko[d], Z. Fraenkel[e], C. Garabatos[b], P. Glässel[c], G. Hering[b], J. Holeczek[b], V. Kushpil[a], B. Lenkeit[g], A. Maas[b], A. Marín[b], F. Messer[f], J. Milošević[c], A. Milov[e], D. Miśkowiec[b], Y. Panebrattsev[d], O. Petchenova[d], V. Petraček[c], A. Pfeiffer[g], J. Rak[b], I. Ravinovich[e], P. Rehak[h], H. Sako[b], W. Schmitz[c], J. Schukraft[g], S. Sedykh[b], W. Seipp[c], S. Shimansky[d], J. Slívová[c], H. J. Specht[c], J. Stachel[c], M. Šumbera[a], H. Tilsner[c], I. Tserruya[e], J. P. Wessels[c], T. Wienold[c], B. Windelband[c], J. P. Wurm[i], W. Xie[e], S. Yurevich[c], V. Yurevich[d]

[a]NPI/ASCR, Řež, Czech Republic
[b]GSI, Darmstadt, Germany
[c]Universität Heidelberg, Germany
[d]JINR, Dubna, Russia
[e]Weizmann Institute, Rehovot, Israel
[f]Department for Physics and Astronomy, SUNY Stony Brook, USA
[g]CERN, Geneva, Switzerland
[h]Brookhaven National Laboratory, Upton, USA
[i]Max-Planck-Institut für Kernphysik, Heidelberg, Germany

1. Introduction

The production of e^+e^--pairs in heavy ion collisions has raised great interest during the last years. Extensive theoretical discussions have been triggered in particular by the CERES measurements of the e^+e^--pair production in 158 AGeV Pb+Au collisions [1]. In the invariant mass region $0.25<m_{ee}<0.7$ GeV/c^2, a significant enhancement of the e^+e^--pair yield compared to the contribution of known hadronic sources was observed. Most of the enhancement is localized in the region of low transverse pair momentum $p_t^{ee}<500$ MeV/c. The threshold behavior of the excess at $\approx 2m_\pi$ together with the multiplicity dependence suggests pion annihilation to be a possible mechanism for additional e^+e^- production. However, the spectral shape of the e^+e^--yield cannot be explained without introducing modifications of the vector meson properties in medium, in particular of the ρ. It has been pointed out that medium modifications of this kind lead to an apparant shift of the hadron-parton duality 'threshold' towards lower masses [2]. The connection between in-medium modifications of meson properties and a possible restoration of chiral

*Supported by: U.S. DoE, German BMBF, the Israeli Science Foundation and the MINERVA Foundation

symmetry has been emphasized since the latter requires the degeneration of all hadronic parity doublets (as the $\rho(770)$ and the $a_1(1260)$) which exist in vacuum [2].

The limited mass resolution of the original CERES spectrometer did not allow for a systematic investigation of possible modifications in the mass region of the narrow resonances ω and ϕ. For that reason the CERES spectrometer has been upgraded by the addition of a new magnet system and a Time Projection Chamber (TPC), to provide a mass resolution on the level of the natural line widths ($\Delta m/m$<2%) [3].

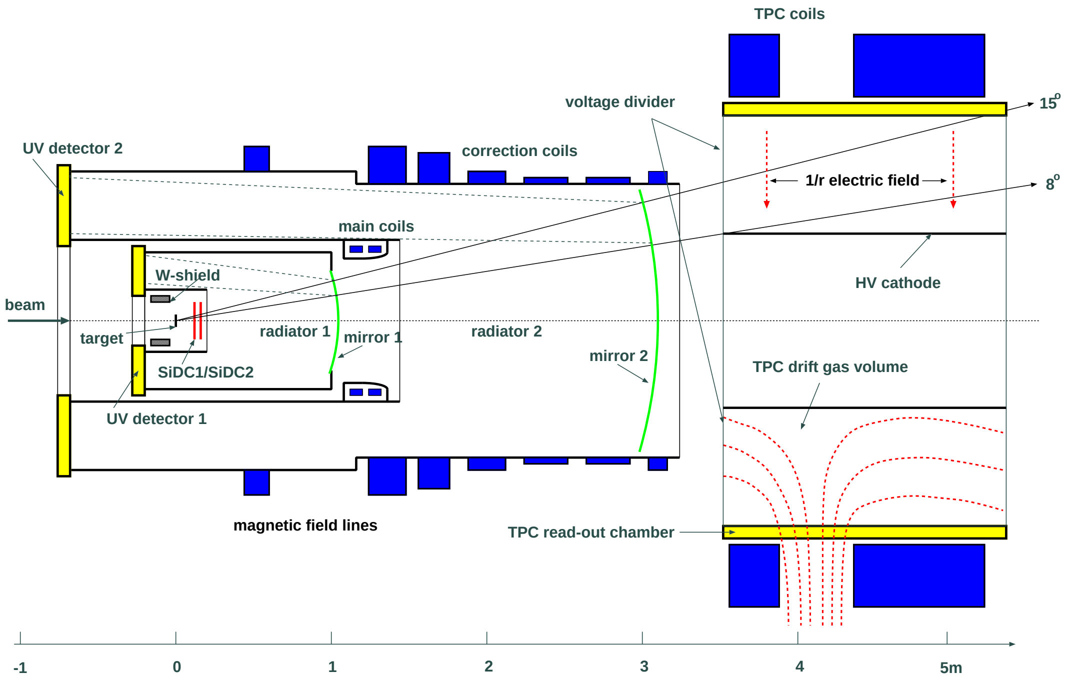

Figure 1. The upgraded CERES spectrometer at the CERN-SPS.

In the fall of 2000 the upgraded CERES spectrometer was operated with a very good overall performance. A sample of 33 M central 158 AGeV Pb+Au events and a smaller set of 0.7 M events at 80 AGeV were recorded. A few preliminary results of this data sample will be presented in this contribution.

We will focus here on results from the 1999 data taking period, where 8 M Pb+Au events at 40 AGeV were recorded. Since the new readout system of the TPC was not yet properly working, this data set is limited in terms of statistics and momentum resolution. Nevertheless, this data sample at lower beam energy allows to study initial conditions different from the ones at top SPS energy. This can be very useful to disentangle temperature and baryon density driven modifications of the dilepton spectrum.

2. Experimental Setup

The CERES spectrometer is dedicated to the measurement of low-mass e^+e^--pairs around midrapidity, providing full azimuthal acceptance in the polar angle region between 8° and 14.5° ($2.1<\eta<2.6$) (Fig.1). The discrimination of rare leptonic signals from the huge hadronic background requires a high electron identification capability. This is provided by two RICH detectors (each consisting of a radiator, a mirror and wire chambers for UV detection) which are operated at high Cherenkov threshold (γ_{th}=32) and are thus insensitive to 95% of the charged hadrons. A precise angle measurement of charged particles and vertex reconstruction is provided by two silicon drift detectors (SiDC1,2) located 10 cm and 11.5 cm behind a segmented Au target. The radial drift TPC has an active length of 2 m and an outer diameter of 2.6 m. It is operated inside a magnetic field with a maximal radial component of 0.5 T and provides the measurement of up to 20 space points for each charged particle track. This allows for a precise determination of the momentum and additional electron ID via dE/dx. The magnet system between the two RICHes was not operated in the upgraded configuration.

3. e^+e^--Pair Analysis

Electrons are identified via their ring signature in the RICH detectors. The absence of magnetic deflection between RICH1 and RICH2 led to an improvement of the ring finding efficiency from 70% to 94%, since ring recognition could now be performed simultaneously in both RICHes. After matching to the SiDC and the TPC, electron tracks are combined to pairs. Only single electron tracks with p_t>200 MeV/c and fully reconstructed pairs with opening angle Θ_{ee}>35 mrad were accepted. The dilepton signal is derived from the number of unlike-sign pairs, subtracting the number of like-sign pairs to account for the combinatorial background. To reduce the combinatorial background arising mainly from unrecognized Dalitz pairs and conversions, further rejection steps have to be taken. The impact of these rejection steps on various subsamples is demonstrated in Fig.2.

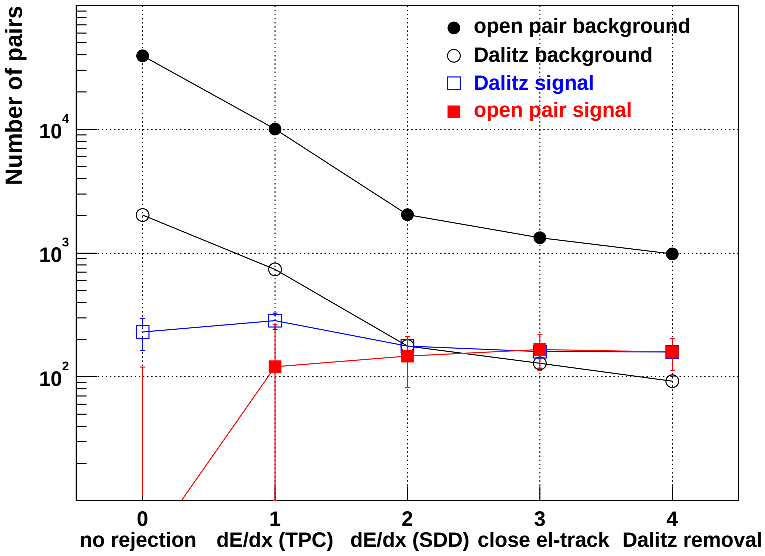

Figure 2. Evolution of the total number of pairs after various rejection steps, shown for the open pair signal (m_{ee}>0.2 GeV/c^2), open pair background (m_{ee}>0.2 GeV/c^2), Dalitz signal (m_{ee}<0.1 GeV/c^2) and Dalitz background (m_{ee}<0.1 GeV/c^2).

First, the electron sample is cleaned from remaining hadronic contaminations, mainly caused by incorrect matches between RICH and TPC. This is done using dE/dx information from the TPC. Conversions and Dalitz pairs which typically have small opening angles leave a clean signature in the SiDC's, because they produce a double energy loss within a small angular region. This allows to reject close pairs (Θ_{ee}<10 mrad) even if they are not recognized as two individual rings in the RICHes. Due to the incomplete azimuthal readout of the TPC in the 1999 data, an additional close track cut (Θ_{ee}<70 mrad) solely based on SiDC-RICH electron candidates was applied. Finally, tracks which combine to a Dalitz pair (m_{ee}<0.2 GeV/c^2) were removed from further combinatorics. By these cuts, the open pair background is reduced by roughly a factor of 40, while the open pair signal remains unchanged, demonstrating that the signal behaves qualitatively different than the background. The total number of open pairs (m_{ee}>0.2 GeV/c^2) is 159$\pm$46 (stat.) at a signal to background ratio of S/B=1/6.

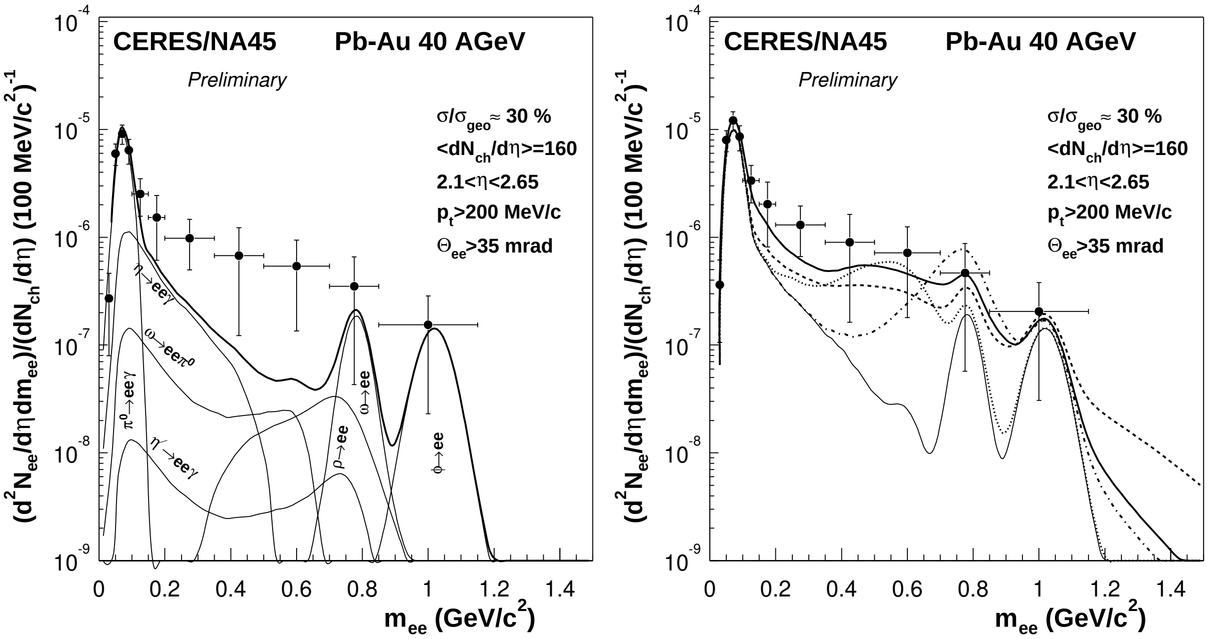

Figure 3. Inclusive e$^+$e$^-$ invariant mass spectrum at 40 AGeV in comparison to expectations from known hadronic sources in heavy ion collisions ('hadronic cocktail') (left) and in comparison to model calculations (right) assuming the vacuum ρ spectral function (dash-dotted), a dropping ρ mass (dotted) and including medium modifications of the ρ spectral function (thick solid line). Also shown is the hadronic cocktail without ρ (thin solid line). The dashed line refers to a lowest order pQCD rate calculation. All calculations are from [4].

The resulting e$^+$e$^-$ invariant mass spectrum was normalized to the hadronic cocktail in the $\pi°$-Dalitz region (Fig.3). Compared to the expectation from known hadronic sources in heavy ion collisions, we observe an enhancement of the e$^+$e$^-$-pair yield by a factor of 4.7$\pm$1.6 (stat.) in the mass range m_{ee}>0.2 GeV/c^2. Most of the enhancement is localized at low transverse pair momentum. This was also observed at 158 AGeV, where, in the same mass range, an enhancement factor of 2.5$\pm$0.4 (stat.) was found. In Fig.3 (right) we compare our result to different model calculations [4]. Clearly the measurement disfavors a purely hadronic scenario assuming the vacuum ρ spectral function, similar to our previous observations at top SPS energy.

4. Hadronic Observables

The addition of the TPC improves substantially the hadron capability of the CERES spectrometer. This allowed for a systematic investigation of hadronic observables around midrapidity. The momentum vector of charged particles is determined from their curvature in the TPC and the emission angle measured in the SiDC. The matching requirement to the SiDC system also leads to a very efficient suppression of non-vertex tracks. The momentum scale of the TPC system has been checked by the width and position of the invariant mass peaks of reconstructed Λ and K°_s hadrons. With the use of the UrQMD model, the multiplicity measurement in the SiDC was related to the corresponding number of participants N_{part}.

4.1. Charged Particle Production and Spectra

The transverse mass distributions of negatively charged hadrons h^- and proton-like positive net charges '$(+)-(-)$' have been measured in different bins of rapidity and centrality. The inverse slope parameters T have been obtained by fitting an exponential $1/m_t\ \mathrm{d}n/\mathrm{d}m_t \propto \exp(-m_t/T)$. In Fig.4 (left) the rapidity averaged results are shown as function of N_{part}. The slopes are similar to those observed at top AGS and SPS energies, with only a weak dependence on centrality. The large difference between h^- and $(+)-(-)$ slopes ($T_{h^-} = 176 \pm 5$ MeV and $T_{(+)-(-)} = 278 \pm 12$ MeV) indicates the presence of strong radial flow also at 40 AGeV. This is only qualitatively reproduced by UrQMD.

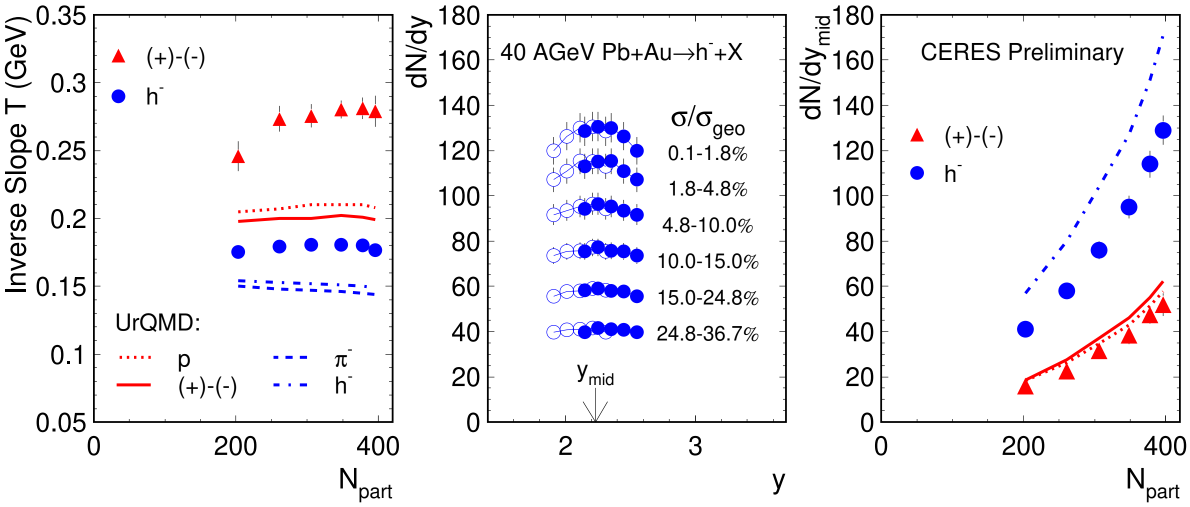

Figure 4. Left: Inverse slope parameters of h^- and $(+)-(-)$ as function of N_{part}. The fit range is $0.1<(m_t-m_\pi)<0.8$ GeV/c^2, $2.2<y_\pi<2.5$ (h^-) and $0.3<(m_t-m_p)<1.5$ GeV/c^2, $2.1<y_p<2.4$ ($(+)-(-)$). Middle: Rapidity density dN/dy of h^- in different centrality bins; open symbols are reflected around midrapidity. Right: The midrapidity yields of h^- and $(+)-(-)$ as function of N_{part}. Also shown are results from UrQMD.

The rapidity densities dN/dy (Fig.4, middle) have been obtained by extrapolating the transverse momentum spectra to p_t=0. The midrapidity yield of h^- as function of N_{part} (Fig.4, right) rises significantly stronger than linear, while a close-to-linear rise at top SPS energy has been reported recently [5]. This points to a change in the particle production mechanism going from 40 AGeV to 158 AGeV. In fact, a non-linear behaviour has also been observed at the AGS [6]. The trend is well described by UrQMD; however, the overall particle production is significantly overestimated. The non-linear rise of the midrapidity $(+)-(-)$-yield with N_{part} is caused by an increasing amount of stopping, in agreement with the UrQMD prediction.

4.2. Two Pion Bose-Einstein Interferometry

The investigation of two-pion Bose-Einstein correlations (HBT) allows a systematic study of the space-time evolution of the hadronic source. We apply a three-dimensional Gaussian parametrization of the correlation function C_2, splitting the three-momentum difference vector into a longitudinal and two transverse components $\vec{q} = (q_{\rm long}, q_{\rm side}, q_{\rm out})$ [7]. Fitting this parametrization to the data yields the correlation strength λ, the homogeneity length parameters $R_{\rm long}$, $R_{\rm side}$, $R_{\rm out}$ and the $R^2_{\rm ol}$ cross-term, the latter being small or consistent with zero in our midrapidity data set. The lack of pion identification leads to a reduction of the correlation strength. However, we expect the shape of the correlation peak to remain unchanged. To account for the finite two-track resolution, only pairs with opening angles $\Theta_{\pi\pi}$>10 mrad were used. All correlation functions have been analyzed in the longitudinal rest frame of the pairs and were corrected for mutual Coulomb repulsion, assuming a finite source size. The relative momentum resolution $\delta q_{\rm long}$ and $\delta q_{\rm side}$ is below 10 MeV/c, leading to only small (<5%) corrections of the fitted source parameters. However, the strong momentum dependence of $\delta q_{\rm out}$ restricts the analysis of $R_{\rm out}$ to small p_t.

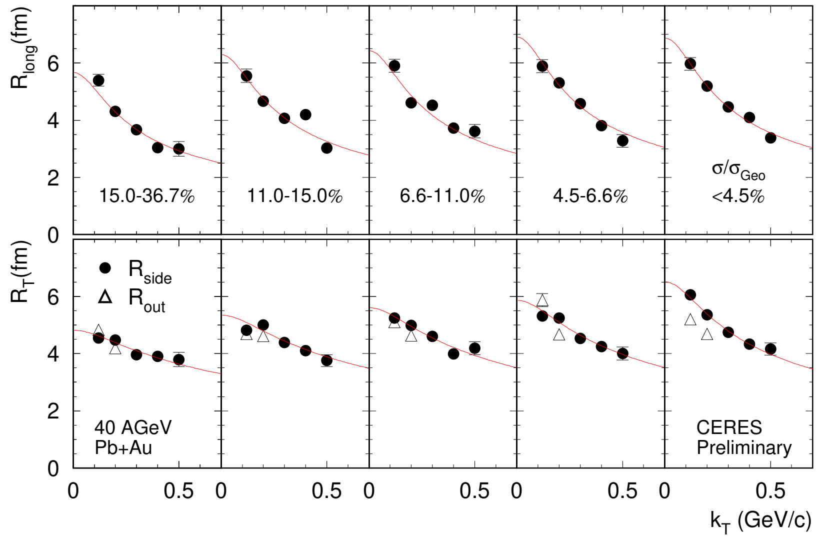

Figure 5. Radius parameters as function of the pair transverse momentum $k_T = \frac{1}{2}|\vec{p_{t,1}} + \vec{p_{t,2}}|$. The range in pair rapidity is $|y_{\pi\pi}\text{-}y_{mid}|<0.25$. Also shown are the fits (see text).

Consistent with the picture of a boost-invariant longitudinal expansion, $R_{\rm long}$ shows a strong k_T dependence in all centrality bins (Fig.5, upper panels). The duration of expansion can be derived [8] by fitting $R_{\rm long} = \tau_0 (T_f/m_T)^{\frac{1}{2}}$, with $m_T = (m_\pi^2 + k_T^2)^{\frac{1}{2}}$. We obtain $\tau_0 = 6 - 7$ fm/c for $T_f = 120$ MeV.

The k_T dependence of $R_{\rm side}$ becomes more pronounced for more central collisions (Fig.5, lower panels), suggesting an increase with centrality of radial flow. We apply a model-dependent parametrization [9] of $R_{\rm side}(k_T)$ which allows to extract the 'true' geometrical source radius $R_{\rm geo}$ and the transverse flow rapidity η_f: $R^2_{\rm side} = R^2_{\rm geo}/(1 + m_T \cdot \eta_f^2/T_f)$. Assuming a Gaussian density profile and a thermal freeze-out temperature of T_f=120 MeV, we obtain from η_f an average transverse flow velocity $\langle\beta_t\rangle = 0.57^{+0.06}_{-0.09}$. A similar result has been obtained from a preliminary HBT analysis of the 80 AGeV data. These numbers are close to the velocity of sound in nuclear medium and similar to findings at top AGS and top SPS energies (Fig.6).

$R_{\rm geo}$ scales with $({\rm d}N/{\rm d}y)^{\frac{1}{3}}$ and is about 7.5 fm for the most central collisions. The freeze-out density can be estimated by $\rho_f = (3 \cdot {\rm d}N^-/{\rm d}y)/(2\pi \cdot R^2_{\rm geo} \cdot \tau_0) \approx 0.12$ pions/fm^3, independent of centrality and identical to results at top SPS and AGS energy [10].

The measured one- and two-particle distributions allow to estimate the spatially averaged phase-space density $\langle f\rangle$ of pions at freeze-out [11]. We observe that $\langle f\rangle$ is consistent with a thermal Bose-Einstein distribution at T=120 MeV independent of centrality (Fig.7). Small deviations from this behaviour at larger p_t can be attributed to the presence of radial flow. Our results support the picture of a universal pion freeze-out phase-space density in heavy-ion reactions at SPS, as already pointed out in [12].

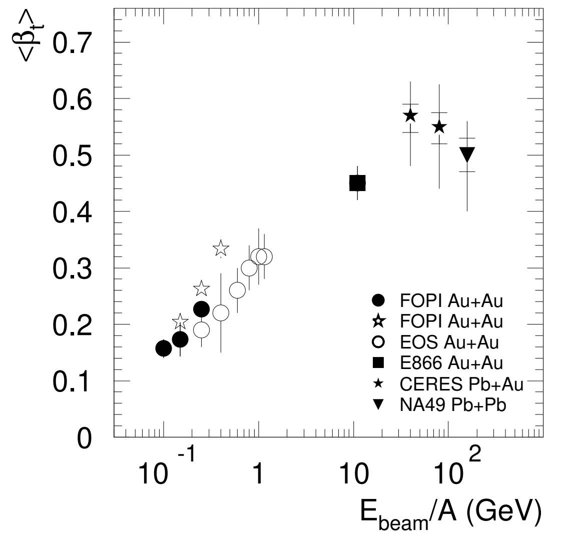

Figure 6. Average transverse flow velocity $\langle\beta_t\rangle$ as function of beam kinetic energy. SPS points are derived from HBT alone, assuming T_f=120 MeV (horizontal marks indicate $\pm$20 MeV uncertainty in T_f).

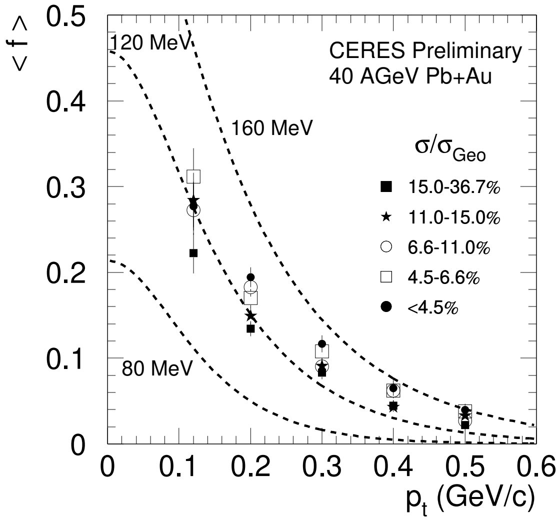

Figure 7. Pion freeze-out phase-space density $\langle f\rangle$ as function of p_t. Also shown are the expectations for static thermal Bose-Einstein distributions at various temperatures.

4.3. Azimuthal Correlations

The investigation of azimuthal correlations ('flow') of charged particles in non-central collisions has been proposed to provide information about the initial pressure in the collision region and the degree of thermalization during the expansion stage.

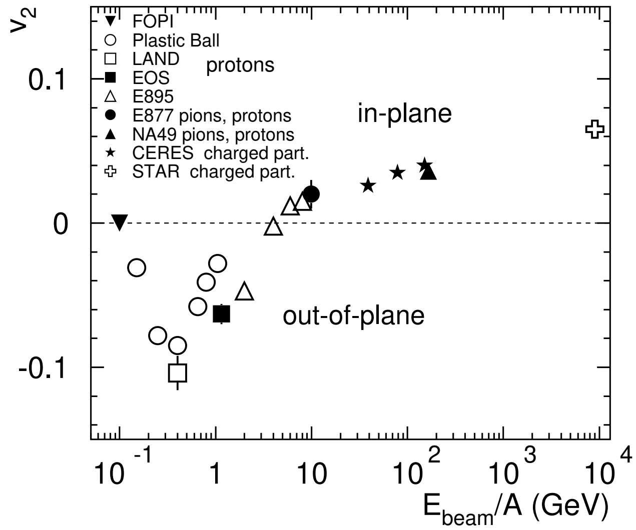

Figure 8. The strength of elliptic flow v_2 as function of the beam kinetic energy for semi-central collisions of Pb or Au nuclei.

A flow analysis of Pb+Au events at 40, 80 and 158 AGeV over a wide range of impact parameters has been performed. This analysis was based on the azimuthal hit distributions in the SiDC1,2. The two coefficients v_1 and v_2, respectively the strength of directed and elliptic flow, are obtained from a second order Fourier decomposition of the relative azimuthal charged particle distribution $dN/d(\phi-\Phi)$ (Φ is the orientation of the reaction plane) [13]. The v_1 and v_2 values have been corrected for the finite reaction plane resolution, determined by the subevent method. While v_1 exhibits the characteristic zero-crossing at midrapidity, v_2 is positive and independent of rapidity within our acceptance. It increases with beam energy and fits smoothly into the measured systematics at different beam energies (Fig.8).

4.4. Mean Transverse Momentum Fluctuations

Fluctuations of the event-wise average transverse momentum $\langle p_t \rangle$ have been predicted as a possible observable for critical phenomena close to the QCD phase boundary [14]. The $\langle p_t \rangle$ distributions of central Pb+Au events at 40, 80, and 158 AGeV are shown in Fig.9 and compared to the corresponding mixed-event distributions. The similarity of real and mixed events suggests that $\langle p_t \rangle$ fluctuations are mainly driven by finite number statistics. A more detailed investigation, however, indicates small additional contributions of order 5 MeV/c to the width of the $\langle p_t \rangle$ distribution, better visualized by the ratio of the real and mixed event distributions (Fig.9, lower panels). Similar results are obtained from an analysis of subevent correlations, as proposed in [15]. The influence of HBT, flow, impact parameter fluctuations and detector efficiency on $\langle p_t \rangle$ are under investigation.

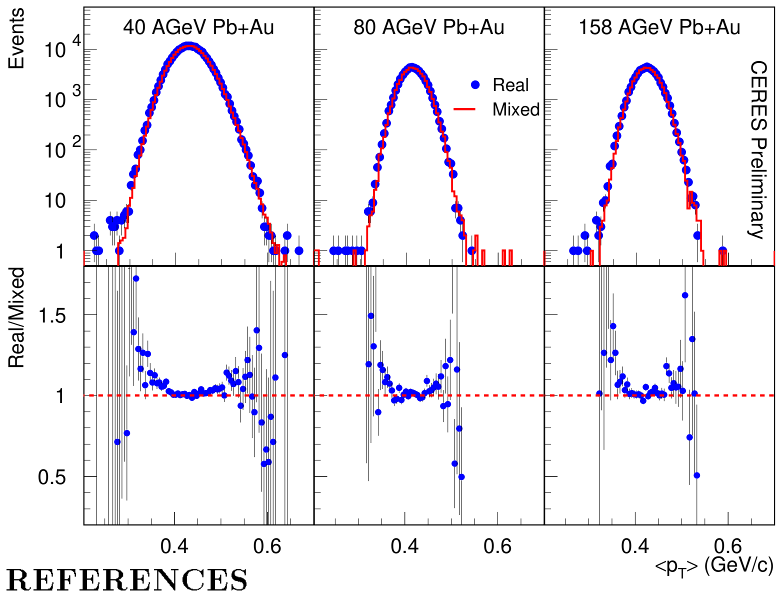

Figure 9. Upper panels: Event-by-event $\langle p_t \rangle$ distributions at three different beam energies. The solid line is obtained by event mixing. Lower panels: Ratio between real and mixed-event distributions. The centrality selection corresponds to σ/σ_{geo}<6.5%. For the calculation of $\langle p_t \rangle$ tracks with 0.05<p_t<1.5 GeV/c were used.

REFERENCES

1. G. Agakichiev et al. (CERES Collaboration), Nucl. Phys. **A661** (1999) 23c.
2. R. Rapp and J. Wambach, Eur. Phys. J. **A6** (1999) 415; R. Rapp, Nucl. Phys. **A661** (1999) 33c; R. Rapp and J. Wambach, hep-ph/9909229.
3. G. Agakichiev et al. (CERES Collaboration), Nucl. Phys. **A661** (1999) 673c.
4. R. Rapp, private communication.
5. M.M. Aggarwal et al. (WA98 Collaboration), Eur. Phys. J. **C18** (2001) 651.
6. L. Ahle et al. (E802 Collaboration), Phys. Rev. **C59** (1999) 2173.
7. G. Bertsch, Nucl. Phys. **A498** (1989) 173c; S. Pratt, Phys. Rev. **D33**, (1986) 1314.
8. Y. Sinyukov, Nucl. Phys. **A498** (1989) 151c.
9. U. Wiedemann, Nucl. Phys. **A661** (1999) 65c.
10. J. Stachel, Nucl. Phys. **A654** (1999) 119c.
11. G. Bertsch, Phys. Rev. Lett. **72** (1996) 2349.
12. D. Ferenc, U. Heinz, B. Tomasik, U. Wiedemann and J.G. Cramer, Phys. Lett. **B457** (1999) 347.
13. S. Voloshin and Y. Zhang, Z. Phys. **C70** (1996) 665.
14. M. Stephanov, K. Rajagopal, E. Shuryak, Phys. Rev. Lett. **81** (1998) 4816.
15. S. Voloshin, NA49 Note number 178 (1999).